Revision 1

Petrogenesis of Chang'E-5 mare basalts: Clues from the trace elements in plagioclase

Heng-Ci Tian[1]*, Wei Yang[1]*, Di Zhang (张棣)[1], Huijuan Zhang[1,3], Lihui Jia[2], Shitou Wu[2], Yangting Lin[1], Xianhua Li[2], Fuyuan Wu[2]

[1]Key Laboratory of Earth and Planetary Physics, Institute of Geology and Geophysics, Chinese Academy of Sciences, Beijing 100029, China

[2] State Key Laboratory of Lithospheric Evolution, Institute of Geology and Geophysics, Chinese Academy of Sciences, Beijing 100029, China

[3] School of Earth Sciences, East China University of Technology, Nanchang 330013, Jiangxi, China

Abstract: 206

Word count: 4217

References: 63

Figures: 7

Revision 1 to AM (Sep 30, 2022)

*Corresponding authors: hctian@mail.iggcas.ac.cn; yangw@mail.iggcas.ac.cn

DOI: https://doi.org/10.2138/am-2022-8570. http://www.minsocam.org/

ABSTRACT

This study focuses on using the chemical compositions of plagioclase to further investigate the petrogenesis of Chang'E-5 young mare basalts and constrain its parental melt composition. Together with previously published data, our results show that the plagioclase in mare basalts overall displays large variations in major and trace element concentrations. Inversion of the plagioclase data indicates that the melt compositions parental to Chang'E-5 basalts have high rare earth elements (REE) concentrations similar to the high-K KREEP rocks (potassium, rare earth elements, and phosphorus). Such a signature is unlikely to result from the assimilation of KREEP components, because the estimated melt Sr shows positive correlations with other trace elements (e.g., Ba, La), which are far from the KREEP endmembers. Instead, the nearly parallel REE distributions and a high degree of trace element enrichment in plagioclase indicate an extensive fractional crystallization process. Furthermore, the estimated melt REE concentrations from plagioclase are slightly higher than those from clinopyroxene, consistent with its relatively later crystallization. Using the Ti partition coefficient between plagioclase and melt, we estimated the parental melt TiO_2 content from the earliest crystallized plagioclase to be ~3.3 wt.%, thus providing robust evidence for a low-Ti and non-KREEP origin for the Chang'E-5 young basalts in the Procellarum KREEP terrane.

Keywords: Plagioclase, clinopyroxene, basalt, low-Ti, rare earth element, KREEP

INTRODUCTION

Lunar basaltic volcanism is the product of partial melting that took place in the lunar mantle and thus provides a window into the thermal and compositional evolution of the Moon's interior (Shearer et al. 2006; Wieczorek et al. 2006). Studies of the lunar samples returned by the Apollo and Luna missions have revealed a large number of clues on the early evolution of the Moon, but less is known about the late Moon. Recently, China's Chang'E-5 mission returned new lunar soils from Oceanus Procellarum that were dated at ca. 2.0 Ga and younger than any Apollo and Luna samples (Che et al. 2021; Li et al. 2021), shedding new light on the late-stage evolution of the Moon. Several studies have reported the petrology, geochemistry and volatile contents of the Chang'E-5 basalts (Che et al. 2021, 2022; Hu et al. 2021; Li et al. 2021; Tian et al. 2021; He et al., 2022; Zhang et al. 2022), as well as the bulk compositions of lunar soils (Li et al., 2022; Zong et al., 2022), suggesting that this basalt represents a new type of rock characterized by a higher FeO (> 22 wt.%) content and a lower Mg# (< 34; =100 × Mg/[Mg + Fe]) compared to the Apollo and Luna samples. The olivine and clinopyroxene crystals in the Chang'E-5 basalts also show lower Mg# than the low-Ti basalts from Apollo 12 and 15 missions. In addition, based on the trace elements in augite, the parental melt compositions estimated by Tian et al. (2021) show high abundances of rare earth elements and incompatible elements (e.g., Zr, Th), similar to KREEP-rich rocks reported in previous studies (e.g., Warren and Wasson 1979; Neal and Kramer 2003; Lin et al., 2012). However, considering the Sr and Nd isotopes, the aforementioned features were unlikely caused by the involvement of a KREEP layer that was formed within the last residual liquid of the postulated Lunar Magma Ocean, but they indicate a depleted mantle source followed by slight partial melting and extensive fractional crystallization (Tian et al. 2021). To date, whether these basalts originate from a low-Ti or high-Ti (i.e., TiO_2 <1 wt.% = very low-Ti; 1-6 wt.% = low-Ti; >6 wt.% = high-Ti; Neal and Taylor 1992) magma source is still debatable. For example, both Tian et al. (2021) and Li et al. (2022) showed that this basalt likely belonged to a low-Ti type by utilizing a more representative sample set and a small fraction of lunar soil, respectively. On the contrary, based on the high-resolution X-ray tomographic microscopy, Jiang et al. (2022) reported a high-Ti composition for a Chang'E-5 basaltic clast that has extremely high ilmenite modal abundance (17.8 vol.%). These different interpretations would have different implications on lunar mantle dynamic processes.

These controversies likely resulted from the commonly small sizes of basaltic fragments (less than < 3mm; Tian et al. 2021; Li et al. 2022), making it difficult to obtain representative whole-rock data. For example, sixteen basaltic clasts investigated by Tian et al. (2021) show a wide range of whole-rock TiO_2 contents varying from 3.0 to 14.3 wt.%. By contrast, plagioclase as a common mineral in lunar rocks could be an effective recorder of the parental melt and crystallization history (e.g., Papike et al. 1994, 1996; Hui et al. 2011; Xu et al. 2020). To further investigate the origin of Chang'E-5 basalts, here we focus on analyzing the major and trace elements in plagioclase and then

This is the peer-reviewed, final accepted version for American Mineralogist, published by the Mineralogical Society of America.
The published version is subject to change. Cite as Authors (Year) Title. American Mineralogist, in press.
DOI: https://doi.org/10.2138/am-2022-8570. http://www.minsocam.org/

"inverting" the data based on the mineral/melt partition coefficients to estimate the compositions of the parental melts from which they formed. This approach can overcome the need for representative whole-rock analyses and reflect the magmatic evolution, and it has been widely used to decipher the petrogenesis of Mg-suite rocks in lunar highlands (e.g., Papike et al. 1994, 1996; Shervais and McGee 1998, 1999; Shearer and Papike 2005; Togashi et al. 2022), ferroan anorthosites (e.g., Papike et al. 1997; Floss et al. 1998; Pernet-Fisher et al. 2019; Xu et al. 2020) and basalts/basaltic breccias (e.g., Hui et al. 2011; Xue et al. 2019). In addition, the inverted melt compositions obtained from plagioclase and clinopyroxene can be compared to see if both data inversions produce concordant melt compositions.

In this work, we obtained major elements of plagioclase from eight Chang'E-5 basaltic clasts that have not been studied before, and trace elements of clinopyroxene and plagioclase from seven of them, as well as one previously studied basaltic clast (406-027,001; Tian et al. 2021). Combing the major and trace element data of plagioclase and pyroxene in previous works and our new data, we estimated the concentrations of REE, Sr, Ba, and Ti, and then discussed the magma evolution and whether the basalt belongs to a low-Ti or high-Ti type.

ANALYTICAL METHODS

We acquired eight new basaltic clasts from a ~2.0 g scooped soil sample (CE5C0400YJFM00406) allocated by the China National Space Administration. These basaltic fragments have sizes between 0.5 × 0.6 mm and 1.1 × 1.4 mm, and they were first embedded in epoxy mounts and then polished using a grinder. Then, we performed the EPMA, LA-ICP-MS, and Raman analyses on plagioclase, K-feldspar, and clinopyroxene. In addition, the clinopyroxene and plagioclase grains from samples studied by Tian et al. (2021) were also analyzed by the Raman spectrometer to examine whether their chemical compositions had been affected by impact processes.

Backscattered electron images (BSE) were obtained by a Thermo scientific Apreo S scanning electron microscope (SEM) housed at the Institute of Geology and Geophysics, Chinese Academy of Sciences (IGGCAS). The epoxy mounts were coated with carbon that has a thickness of ~20 nm. To acquire high-quality images, the CBS detector was used and the operating conditions of the instrument were set as 15.0 kV and 6.4 nA. After the SEM analysis, major and minor element concentrations of plagioclase and K-feldspar were acquired by a JEOL JXA8100 electron probe at the IGGCAS. The operating accelerating voltage was 15 kV and the beam current was 20 nA. Calibration of the data was done by using a series of natural minerals and synthetic materials. Based on the analysis of internal laboratory standards, the precision for major (> 1.0 wt.%) and minor (< 1.0 wt.%) elements are better than 1.5% and 5.0%, respectively. Plagioclase from eight samples was randomly selected and analyzed. The EPMA data for plagioclase and K-feldspar are provided in Online Materials[1] Table OM1.

Trace element abundances of clinopyroxene and plagioclase were measured by LA-ICP-MS employing an Element XR HR-ICP-MS instrument (Thermo Fisher

Scientific, USA) coupled to a 193 nm ArF excimer laser system (Geolas HD, Lambda Physik, Göttingen, Germany) at the IGGCAS, following the procedures reported in a previous study (Wu et al. 2018). The laser diameter was ~32 μm with a repetition rate of 3 Hz. The laser energy density was ~3.0 J/cm^2. The analytical spots were in the cores of relatively large euhedral plagioclase grains. The Element XR is equipped with a high-capacity interface pump (OnTool Booster 150, Asslar, Germany) in combination with a Jet sample and normal H-skimmer cones to achieve a detection efficiency in the range of 1.5%. The NIST SRM 610 (Jochum et al. 2011) and ARM-1 (Wu et al. 2019) reference materials were used for external calibration. The analytical uncertainties for most trace elements (> 0.05 ppm) are better than 10% (relative standard deviation). In addition, this LA-ICP-MS technique can simultaneously obtain the major element contents for the same spots, and the precision and accuracy for major elements are better than 5% (relative deviation). These major element data were used to calculate the anorthite contents. During our analysis, two international glass standards were analyzed (BCR-2G and GOR132-G) and the results agree with the recommended values (Online Materials[1] Table OM2).

We carried out Raman spectroscopic analysis to investigate whether plagioclase and clinopyroxene were affected by impact processes. Raman spectrum was collected with a Confocal Raman Microscope alpha 300R made by WITec GmbH (Ulm, Germany) at the IGGCAS. This system is equipped with a solid-state continuous-wave laser emitting at 532 nm, which is fiber coupled to the instrument (Gao et al. 2020). Single-crystal silicon was used to correct the wavenumbers of the shifts. A 50× ZEISS objective was selected for excitation and detection. The laser energy was set to 7 mW, and the acquisition time was 2s with an accumulation of 3.

RESULTS

The major chemical compositions of plagioclase and K-feldspar from Chang'E-5 basaltic clasts obtained by EPMA are reported in Online Materials[1] Table OM1. The major and trace elemental concentrations of clinopyroxene and plagioclase obtained by LA-ICP-MS are given in Online Materials[1] Tables OM3 and OM4. In addition, the location of analytical spots and traverses are shown in the BSE images (Online Materials[1] Figs. OM1 and OM2). In terms of the textures, the eight new samples include two subophitic, one poikilitic, one porphyritic and four coarse-grained fragments (Online Materials[1] Figs. OM1 and OM2). Similar to previous studies, these basalts are mainly composed of clinopyroxene, plagioclase, olivine and ilmenite, with minor spinel, silica and sulfides (Online Materials[1] Figs. OM1 and OM2). The plagioclases exhibit a large variation in anorthite composition from $An_{7.9}$ to $An_{90.3}$ (Ca/[Ca + Na +K], mole percent) based on the EPMA analysis (Figure 1). The K-feldspar grains are commonly anhedral and occur in the interstitial mesostasis. These samples have K_2O contents ranging from 0.04 to 7.63 wt.% and low TiO_2 contents from 0.03 to 0.84 wt.% (Online Materials[1] Table OM1). Several measured TiO_2 contents were below the EPMA detection limits (~90 ppm for Ti) and thus excluded in the following discussion. The new data obtained in this study,

This is the peer-reviewed, final accepted version for American Mineralogist, published by the Mineralogical Society of America.
The published version is subject to change. Cite as Authors (Year) Title. American Mineralogist, in press.
DOI: https://doi.org/10.2138/am-2022-8570. http://www.minsocam.org/

combined with the available data of Chang'E-5 samples (Che et al. 2021; Hu et al. 2021; Tian et al. 2021), exhibit a negative correlation between K_2O and An contents (Figure 1b), but no correlation between TiO_2 and An contents (Figure 1c). These geochemical characteristics show a high degree of similarity to those of the Apollo low-Ti basalts (Figure 1).

In the chondrite-normalized element diagrams, all plagioclase grains analyzed by LA-ICP-MS are rich in light rare earth elements (LREE) relative to the heavy rare earth elements (HREE), with La ~2× to ~30× chondrite, the HREE ~0.1× to ~1× chondrite and also have clear positive Eu anomalies (Figure 2). No appreciable trace elemental differences were found in the plagioclases for different textural fragments. Additionally, the analyzed plagioclase grains also have high abundances of Sr (574-1990 ppm) and Ba (73-1208 ppm), and the measured concentrations of La, Ba, Eu and Sr gradually increase with a decreasing An content acquired by LA-ICP-MS (Figure 3). As expected, clinopyroxene is LREE-depleted with a deep negative Eu anomaly, which overlaps with that of the other fragments reported in Tian et al. (2021) (Figure 2e). Similar to plagioclase, clinopyroxene also shows highly variable and parallel REE patterns (Figure 2e), indicating their compositional variations were likely controlled by the same process.

The Raman results show that the pyroxene and plagioclase, including those that have been analyzed for trace elements in Tian et al. (2021) and this work, preserve their typical shape and peak positions (663-673 and 998-1012 cm^{-1} for pyroxene, and 483-489 and ~508 cm^{-1} for plagioclase; Figure 4 and Online Materials[1] Fig. OM3).

DISCUSSION

Evaluation of post-magmatic processes

Before we invert the measured data to estimate the parental melt compositions, we should carefully evaluate the effects of magmatic and post-magmatic processes on the compositions of plagioclase. A previous study by Papike et al. (1996) reported small differences in REE distributions between the melts estimated from pigeonite and plagioclase in Mg-suite norites, which might have resulted from re-equilibration with LREE diffusing into plagioclase and HREE diffusing into pigeonite during slow subsolidus cooling. This re-equilibrium process in fact did not have a significant influence on the results of the estimated melt compositions (e.g., Papike et al. 1996; Shervais and McGee 1999). Compared to these intrusive rocks, the Chang'E-5 basalts are extrusive products and they are expected to cool down quickly on the lunar surface. In the diagram of the pyroxene thermometer, the pyroxene cores recorded an equilibrium temperature of ~1,000-1,200 °C (Fig. 2c in Tian et al. 2021), while the rims reflected much lower temperatures of less than 800 °C. The large temperature changes from the core to the rims imply a rapid cooling process. In addition, the diffusion of Sr, Ba and Ti in plagioclase is also very slow due to their high charge and large ionic radius (Cherniak and Watson 1994; Cherniak 2002; Druitt et al. 2012). For example, Togashi et al. (2017) suggested that plagioclase in ferroan anorthosites retains near-primary concentrations of Sr and Ti, in contrast to Mg, which appears to be partially re-equilibrated by diffusion

DOI: https://doi.org/10.2138/am-2022-8570. http://www.minsocam.org/

during magmatic processes. On the other hand, the lunar surface has been subjected to periods of meteoroid impacts over geological time (e.g., Stöffler et al. 2006; Norman 2009). Strong chemical modification can occur as the result of localized diffusional mechanics during shock-induced thermal metamorphism (Phinney 1991). Pernet-Fisher et al. (2017) used Fourier transform infrared spectroscopy approach to estimate the impacts on the influence of trace-element systematics of plagioclase in ferroan anorthosites. The authors found weak correlations between plagioclase shock state and trace elemental ratios (e.g., La/Y, Sm/Nd), implying that shocks could redistribute some trace elements. The shock-melt zones and maskelynite phase were found in Chang'E-5 basalts (Che et al. 2021), suggesting that the basaltic clasts were influenced by shocks. In this study, basaltic fragments that have no obvious shock-induced regions were chosen for chemical analyses. Our Raman results show that the plagioclase and clinopyroxene analyzed for trace elements in both our earlier work (Tian et al. 2021) and this work were not modified by shocks (Figure 4; Online Materials[1] Fig. OM3). According to these pieces of evidence, we conclude that the plagioclase cores could provide reliable estimates of parental melt compositions (e.g., Papike et al. 1996; Shervais and McGee 1999; Togashi et al. 2022).

Calculation of equilibrium parental magma

The trace element partitioning between plagioclase and silicate melts has been investigated previously in a wide range of experimental conditions (e.g., Mckay 1982; Phinney and Morrison 1990; Blundy and Wood 1991; Bindeman et al. 1998; Bindeman

DOI: https://doi.org/10.2138/am-2022-8570. http://www.minsocam.org/

and Davis 2000; Aigner-Torres et al. 2007; Sun et al. 2017), where they found that the partition coefficients (D) are related to the An content and temperature (e.g., Blundy and Wood 1991; Sun et al. 2017). In this work, we used the lattice strain models described in Sun et al. (2017) instead of the empirical equations (e.g., Blundy and Wood 1991; Bindeman et al. 1998) to estimate the parental melt compositions:

$$D_j = D_0 exp[\frac{-4\pi E N_A}{RT}(\frac{r_0}{2}(r_0 - r_j)^2 - \frac{1}{3}(r_0 - r_j)^3)] \quad (1)$$

where D_0 is the strain-free partition coefficient; r_j is the ionic radius; r_0 is the ionic radius of the strain-free lattice site; E is the effective Young's modulus; and N_A is the Avogadro constant. The three lattice strain parameters (D_0, r_0, and E) as a function of temperature, pressure and composition can be obtained using the following expressions that are determined for trivalent element (REE+Y) in plagioclase:

$$\ln D_0^{3+} = 16.05(\pm 1.57) - \frac{19.45(\pm 1.78)+1.17(\pm 0.14)P^2}{RT} \times 10^4 - 5.17(\pm 0.37)(X_{Ca})^2 \quad (2)$$

$$r_0^{3+}(\text{Å}) = 1.179(\pm 0.027) \quad (3)$$

$$E^{3+}(GPa) = 196(\pm 51) \quad (4)$$

where X_{Ca} is the Ca content in plagioclase per eight-oxygen; P is pressure in GPa; and numbers in parentheses refer to 2σ uncertainties. Similarly, the lattice strain model was also chosen to predict the trace element concentrations of melt equilibrium with pyroxene. Because most of the analyzed pyroxene grains in this work and Tian et al. (2021) belong to high-Ca pyroxene (Wo > 25; Online Materials[1] Table OM3), the expressions suitable for Fe-rich high-Ca pyroxene were used to obtain lattice strain parameters (D_0, r_0, and E) (see Dygert et al. 2014 for more details).

The calculated partition coefficients for plagioclases and high-Ca pyroxene are listed in Table 1. Figure 5 shows the calculated, chondrite-normalized REE concentrations of parental melts estimated from both the high-Ca pyroxene and plagioclase. We find that the melts estimated from plagioclase largely overlap the field of the melts estimated from high-Ca pyroxene, both of which are higher than those of the Apollo 12 and 15 low-Ti samples. These two fields also cover the range of the A15 KREEP-rich basalts, suggesting that the melts parental to the Chang'E-5 basalts are highly enriched in incompatible elements. Despite of the large overlap, the average REE concentrations of the estimated melt from plagioclase are about 1-2 times higher than those of the melt estimated from high-Ca pyroxene (Figure 5). The different parental melt compositions recorded by pyroxene and plagioclase may have resulted from fractional crystallization. The REEs mostly behave as incompatible elements during basaltic magma differentiation, and the residual melt would be expected to have higher REE concentrations with increasing magmatic differentiation. Using the PETROLOG software, Zhang et al. (2022) modelled the fractional crystallization scenario and showed that plagioclase became a liquidus phase slightly later than pyroxene regardless of a low-Ti or high-Ti magma source. In addition, we note that the REE concentrations of Chang'E-5 lunar soils (Li et al. 2022; Zong et al. 2022) and impact glass beads (Yang et al. 2022) fall on the lower end of the calculated parent melts from both high-Ca pyroxene and plagioclase (Figure 5), although the coefficients derived from lattice strain model is relatively accurate. The discrepancy suggests that we may overestimate the concentrations of REE in the parental

DOI: https://doi.org/10.2138/am-2022-8570. http://www.minsocam.org/

melt, which may derive from the uncertainties in the REE partitioning model, temperature, pressure and chemical compositions used in the calculation. As such, care should be taken when we chose appropriate model and parameters. Nevertheless, this result still suggests that most of the crystallized plagioclases would record a more evolved melt composition, consistent with its higher REE concentrations compared to the melt estimated from pyroxene (Figure 5).

The enrichment of incompatible elements has been found in both lunar samples and meteorites, such as lunar meteorite NWA 773 (Borg et al. 2004), 15386 KREEP basalt (Neal and Kramer 2003) and A14/A15 Mg-suite rocks (Papike et al. 1994, 1996). These geochemical characteristics are generally considered to be to the KREEP component that may has been added to the magmas by assimilation during magma ascent or mixing into the mantle source (e.g., Papike et al. 1994; Shearer and Papike 2005; Neal and Kramer 2006). However, several observations suggest that the enrichment of incompatible elements in Chang'E-5 basalts was likely formed through a large degree of fractional crystallization from a liquid that represented a small degree of partial melting of the original source, rather than by assimilating KREEP-rich components. First, both the high-Ca pyroxene and plagioclase phases from different textured basalts show large chemical variations but parallel REE distributions (Figure 2), consistent with products of fractional crystallization. Second, based on the comparison between An contents and some trace elements (e.g., Sr, Ba, La and Eu), the negative non-linear correlations and the 10 times increase of trace element concentrations imply that the plagioclase recorded a gradual enrichment of incompatible elements in the parental melt (Figure 3). Third, the estimated melts from plagioclase exhibit much higher Sr concentrations (338-1221 ppm) than the KREEP (~200 ppm; Warren, 1989) and lunar crust (~143-234 ppm; represented by Apollo 16 lunar anorthosites; Pernet-Fisher et al. 2019) (Figure 6). The Sr concentrations of parental melts are positively correlated with Ba, La and Eu concentrations, which are far from the KREEP endmember (Figure 6). Finally, it should be noted that young lunar basaltic meteorites, such as NWA 4734, 032 and LAP 02205 with an age of ~3.0 Ga, were also thought to be unrelated to the KREEP materials (Elardo et al. 2014, and references therein). Therefore, we conclude that KREEP is not a prerequisite for most partial melting within the lunar interior.

The Rima Sharp, the longest lunar sinuous rille on the Moon, may have fed lava flows to the Chang'E-5 landing site, and the volcanic vent is at least 100 km far from the landing site (Qian et al. 2021). The lava flows, which had open channels connecting the vents to the flow fronts after their emplacement on the lunar surface, could have potentially eroded the underlying regolith during the movement and then incorporated them into the lave flows, as previously documented in Apollo 12 and 14 basalt samples (e.g., Dungan and Brown 1977; Hui et al. 2011). The samples investigated here, however, do not show obvious evidence for the presence of assimilation because most data follow the fractional crystallization trajectory. Future studies on more diverse lunar samples are needed to better understand whether the underlying regoliths were involved in lava flows, which could also provide insights into the chemical compositions of the underlying rocks.

Estimated TiO_2 contents for the parental melt

The TiO_2 contents of plagioclase are also critical to determining whether the basalt originated from a low-Ti or high-Ti magma source. Unlike the inverted-V shape distribution of Ti concentrations with Fo values shown by olivine grains (Fig. 4 in Zhang et al. 2022), the TiO_2 concentrations in our studied plagioclase acquired by EPMA do not show an apparent correlation with An (Figure 1c), which were possibly due to the lack of plagioclase with An contents between ~20 and ~70. These plagioclase data from different textured clasts overlap with each other significantly, similar to the plagioclase from Apollo 12 and 15 low-Ti basalts (Figure 1c). To accurately calculate the magma TiO_2 contents, the choice of the proper partition coefficient between plagioclase and melt is important for the modelling. Similar to other elements mentioned above, previous studies have also shown that Ti partitioning between plagioclase and melt has a strong dependence on An fraction and temperature (e.g., Bindeman et al. 1998; Bindeman and Davis 2000; Aigner-Torres et al. 2007; Tepley et al. 2010; Nielson et al. 2017). To minimize the effect of temperature and melt composition on $D_{Ti\text{-}plag/melt}$, we used basaltic to basaltic-andesitic melts to calculate the $D_{Ti\text{-}plag/melt}$ values because their compositions are similar to our samples with a weighted mean SiO_2 content of about 42.1 wt.% (Tian et al. 2021). Togashi et al. (2022) recently summarized the experimental data and obtained two exponential equations for Ti partitioning: $\text{In}D_{Ti\text{-}plag/melt} = -2.93 \times X_{An} -1.12$ (averaged model) and $\text{In}D_{Ti\text{-}plag/melt} = -4.47 \times X_{An} -0.312$ (low model). Using these calculated partition coefficients, they estimated the compositions of the host magma of Apollo 12 and 14 plutonic rocks. In this study, we applied the first equation to calculate the partition coefficient, given that the second equation was derived by the comparison of plagioclase data and whole-rock data from the same sample.

The estimated TiO_2 concentrations for each data point are shown in Figure 7a, and the melts overall have TiO_2 contents similar to those of the Apollo low-Ti basalts but lower than the melts estimated from Apollo high-Ti basalts. Since the different Chang'E-5 basaltic clasts were expected to share a common source (Li et al. 2021; Tian et al. 2021; Zhang et al. 2022), we calculated average TiO_2 contents for ΔAn = 1 to represent the average parental melt compositions. We have found that the TiO_2 content of parental melt inverted from the most primitive plagioclase (An = ~ 90) is about 3.3 ± 0.4 wt.% (1SD; Figure 7b), which falls into the low-Ti range (Neal and Taylor 1992). This estimated TiO_2 content is slightly lower than the estimated TiO_2 value from olivine (~4.4 wt.%). One possible explanation for this discrepancy could be that the Ti partition coefficient between olivine and melt used in Zhang et al. (2022) was underestimated, which was also noted in their work. With the decrease of An, TiO_2 contents increase a little from ~3.3 ± 0.4 wt.% at An = 90 to ~5.7 ± 5.1 wt.% at An = ~82, implying the presence of continuous crystallization of mafic minerals rather than ilmenite during this stage. This inference is consistent with the texture that ilmenite represents a late-stage crystallization phase since they commonly cut the matrix plagioclase and pyroxene (Tian et al. 2021). From this perspective, the late crystallization of ilmenite also supports a low-Ti origin because ilmenite would be an early crystallized mineral in high-Ti magma (Neal et al. 1990; Simon and Sutton 2018). These observations thus indicate differentiation of a low-Ti magma source rather than a high-Ti magma source. Collectively, compared to the large variation of whole-rock TiO_2 contents (3.0-14.3 wt.%; Che et al. 2021; Tian et al. 2021), the relatively consistent/less variable plagioclase composition provides more convincing evidence of the magma source nature and records their igneous crystallization history.

IMPLICATIONS

Even though the studied basaltic fragments experienced meteoroid impacts and solar wind radiation since ~2.0 Ga (Che et al. 2021; Li et al. 2021), the cores of plagioclase and pyroxene still retain reliable trace element records of their igneous crystallization history and source compositions. The chemical compositions of minerals can not only provide important constraints on the average compositions of the bulk rock, but also record the magmatic evolutionary pathways from which they formed. The data presented here suggest that the average melt REE concentrations, calculated by the inversion of both the clinopyroxene and plagioclase data, are similar to the high-K KREEP, and they are likely to form by a high degree of fractional crystallization rather than assimilation of KREEP materials. Our study on trace elements in plagioclase and the previous study on the Chang’E-5 olivine (Zhang et al. 2022) have confirmed and demonstrated that the Chang’E-5 basalts originated from a low-Ti magma source. This conclusion implies that the high-Ti basalts reported in Chang'E-5 soils may represent the sampling bias because of their small size. Nevertheless, we cannot rule out the possibility that the high-Ti basaltic fragments were the ejected materials from other craters (Xie et al. 2020; Liu et al. 2021).

ACKNOWLEDGEMENTS AND FUNDING

We thank the China National Space Administration for providing the lunar soil samples. We would like to thank the AE Claire Bucholz and an anonymous reviewer for their constructive comments, which greatly improved the manuscript. We are also grateful to Dr. Jun Du for valuable suggestions. This work was supported by the Key Research program of Chinese Academy of Sciences (ZDBS-SSW-JSC007-15), the pre-research project on Civil Aerospace Technologies of China National Space Administration (D020203), the Strategic Priority Research Program of Chinese Academy of Sciences (XDB 41000000), the key research program of the Institute of Geology and Geophysics, Chinese Academy of Sciences (IGGCAS-202101) and the Youth Innovation Promotion Association of the Chinese Academy of Sciences (2022064).

REFERENCES CITED

Aigner-Torres, M., Blundy, J., Ulmer, P., and Pettke, T. (2007) Laser Ablation ICPMS study of trace element partitioning between plagioclase and basaltic melts: an experimental approach. Contributions to Mineralogy and Petrology, 153, 647-667.

Anders, E., and Grevesse, N. (1989) Abundances of the elements: Meteoritic and solar. Geochimica et Cosmochimica Acta 53, 197-214.

Bindeman, I.N., and Davis, A.M. (2000) Trace element partitioning between plagioclase and melt: investigation of dopant influence on partition behavior. Geochimica et Cosmochimica Acta, 64, 2863-2878.

Bindeman, I.N., Davis, A.M., and Drake, M.J. (1998) Ion microprobe study of plagioclase-basalt partition experiments at natural concentration levels of trace elements. Geochimica et Cosmochimica Acta, 62, 1175-1193.

Blundy, J.D., and Wood, B.J. (1991) Crystal-chemical controls on the partitioning of Sr and Ba between plagioclase feldspar, silicate melts, and hydrothermal solutions. Geochimica et Cosmochimica Acta, 55, 193-209.

Borg, L.E., Shearer, C.K., Asmerom, Y., and Papike, J.J. (2004) Prolonged KREEP magmatism on the Moon indicated by the youngest dated lunar igneous rock. Nature 432, 209-211.

Che, X.C., Nemchin, A., Liu, D.Y., Long, T., Wang, C., Norman M.D., Joy K.H., Tartèse, R., Head, J., Jolliff, B., Snape, J.F., Neal, C.R., Whitehouse, M.J., Crow, C., Benedix, G., Jourdan, F., Yang, Z., Yang, C., Liu, J.H., Xie, S.W., Bao, Z.M., Fan, R.L., Li, D.P., Li, Z.S., and Webb S.G. (2021) Age and composition of young basalts on the Moon, measured from samples returned by Chang'e-5. Science, 374, 887-890.

Che, X.C., Snape, J.F., Tartèse, R., Head, J., Jolliff, B., Joy K.H., Long, T., Nemchin, A., Norman M.D., Neal, C.R., Xie, S.W., Whitehouse, M.J., Bao, Z.M., Shi, Y., and Liu, D.Y. (2022) Mineralogy and petrology of basaltic fragments in Channg'E-5 sample CE5C0400. 53rd Lunar and Planetary Science Conference, Abstract 1362.

Cherniak, D.J. (2002) Ba diffusion in feldspar. Geochimica et Cosmochimica Acta, 66, 1641-1650.

Cherniak, D.J., and Watson, E.B. (1994) A study of strontium diffusion in plagioclase using Rutherford backscattering spectroscopy. Geochimica et Cosmochimica Acta, 58, 5179-5190.

Druitt, T.H., Costa, F., Deloule, E., Dungan, M., and Scaillet, B. (2012) Decadal to monthly timescales of magma transfer and reservoir growth at a caldera volcano. Nature, 482, 77-80.

Dungan, M.A., and Brown, R.W. (1977) The petrology of the Apollo 12 ilmenite basalt suite. Proceedings of lunar and planetary science, 8, 1339-1381.

Dygert, N., Liang, Y., Sun, C., and Hess, P. (2014) An experimental study of trace element partitioning between augite and Fe-rich basalts. Geochimica et Cosmochimica Acta, 132, 170-186.

Elardo, S.M., Shearer, C.K., Fagan, A.L., Borg, L.E., Gaffney, A.M., Burger, P.V., Neal, C.R., Fernandes, V.A., and McCubbin, F.M. (2014) The origin of young mare basalts inferred from lunar meteorites Northwest Africa 4734, 032, and LaPaz Icefield 02205. Meteoritics & Planetary Science, 49, 261-291.

Floss, C., James, O.B., McGee, J.J., and Crozaz, G. (1998) Lunar ferroan anorthosite petrogenesis: Clues from trace element distributions in FAN subgroups. Geochimica et Cosmochimica Acta, 62, 1255-1283.

Gao, J., Wu, W., Jia, L., Wang, C.P., Liu, Y., Xu, C., Chen, F., Fei, C., and Su, W. (2020) Raman and infrared spectra to monitor the phase transition of natural kyanite under static compression. Journal of Raman Spectroscopy, 51, 2102-2111.

He, Q., Li, Y., Baziotis, I., Qian, Y., Xiao, L., Wang, Z., Zhang, W., Luo, B., Neal, C.R., James, D., Pan, F., She, Z., Wu, X., Hu, Z., Zong, K and Wang, L. (2022). Detailed petrogenesis of the unsampled Oceanus Procellarum: The case of the Chang'e-5 mare basalts. Icarus, 383, 115082.

Hu, S., He, H.C., Ji, J.L., Lin, Y.T., Hui, H.J., Anand, M., Tartèse, R., Yan, Y.H., Hao, J.L., Li, R.Y., Gu, L.X., Guo, Q., He, H.Y., and Ouyang, Z.Y. (2021) A dry lunar mantle reservoir for young mare basalts of Chang'e-5. Nature, 600, 49-53.

Hui, H.J., Oshrin, J.G., and Neal, C.R. (2011) Investigation into the petrogenesis of Apollo 14 high-Al basaltic melts through crystal stratigraphy of plagioclase. Geochimica et Cosmochimica Acta, 75, 6439-6460.

Jiang, Y., Li, Y., Liao, S., Yin, Z., and Hsu, W. (2022) Mineral chemistry and 3D tomography of a Chang'E 5 high-Ti basalt: implication for the lunar thermal evolution history. Science Bulletin, 67, 755-761.

Jochum, K.P., Weis, U., Stoll, B., Kuzmin, D., Yang, Q., Raczek, I., Jacob, D.E., Stracke, A., Birbaum, K., Frick, D.A., Günther, D., and Enzweiler, J. (2011) Determination of reference values for NIST SRM 610–617 glasses following ISO guidelines.

Geostandards and Geoanalytical Research, 35, 397-429.

Li, C.L., Hu, H., Yang, M.F., Pei, Z.Y., Zhou, Q., Ren, X., Liu, B., Liu, D., Zeng, X., Zhang, G., Zhang, H., Liu, J., Wang, Q., Deng, X., Xiao, C., Yao, Y., Xue, D., Zuo, W., Su, Y., Wen, W. and Ouyang, Z. (2022) Characteristics of the lunar samples returned by the Chang'E-5 mission. National Science Review, 9, nwab188.

Li, Q.L., Zhou, Q., Liu, Y., Xiao, Z., Lin, Y., Li, J.H., Ma, H.X., Tang, G.Q., Guo, S., Tang, X., Yuan, J.Y., Li, J., Wu, F.Y., Ouyang, Z., Li, C., and Li, X.H. (2021) Two-billion-year-old volcanism on the Moon from Chang'e-5 basalts. Nature, 600, 54-58.

Liu, T.T., Michael, G., Zhu, M.H., and Wünnemann, K. (2021) Predicted sources of samples returned from Chang'e-5 landing region. Geophysical Research Letters, 48.

Lin, Y., Shen, W., Liu, Y., Xu, L., Hofmann, B.A., Mao, Q., Tang, G.Q., Wu, F., and Li, X.H. (2012) Very high-K KREEP-rich clasts in the impact melt breccia of the lunar meteorite SaU 169: New constraints on the last residue of the Lunar Magma Ocean. Geochimica et Cosmochimica Acta, 85, 19-40.

Mckay, G.A. (1982) Partitioning of REE between olivine, plagioclase, and synthetic basaltic melts: implications for the origin of lunar anorthosites. Lunar and Planetary Science Conference, 13, 493-494.

Neal, C.R., and Kramer, G.Y. (2003) The composition of KREEP: A detailed study of KREEP basalt 15386. 34th Lunar and planetary Science Conference, Abstract, 2023.

Neal, C.R., and Kramer, G.Y. (2006) The petrogenesis of the Apollo 14 high-Al mare basalts. American Mineralogist, 91, 1521-1535.

Neal, C.R., and Taylor, L.A. (1992) Petrogenesis of mare basalts: A record of lunar volcanism. Geochimica et Cosmochimica Acta, 56, 2177-2211.

Neal, C.R., Taylor, L.A., Hughes, S.S., and Schmitt, R.A. (1990) The significance of fractional crystallization in the petrogenesis of Apollo 17 Type A and B high-Ti basalts. Geochimica et Cosmochimica Acta, 54, 1817-1833.

Nielsen, R.L., Ustunisik, G., Weinsteiger, A.B., Tepley Iii, F.J., Johnston, A.D., and Kent, A.J.R. (2017) Trace element partitioning between plagioclase and melt: An investigation of the impact of experimental and analytical procedures. Geochemistry, Geophysics, Geosystems, 18, 3359-3384.

Norman, M.D. (2009) The Lunar Cataclysm: Reality or “Mythconception”? Elements, 5, 23-28.

Papike, J.J., Fowler, G.W., and Shearer, C.K. (1994) Orthopyroxene as a recorder of lunar crust evolution: An ion microprobe investigation of Mg-suite norites. American Mineralogist, 79, 796-800.

Papike, J.J., Fowler, G.W., and Shearer, C.K. (1997) Evolution of the lunar crust: SIMS study of plagioclase from ferroan anorthosites. Geochimica et Cosmochimica Acta, 61, 2343-2350.

Papike, J.J., Fowler, G.W., Shearer, C.K., and Layne, G.D. (1996) Ion microprobe investigation of plagioclase and orthopyroxene from lunar Mg-suite norites: Implications for calculating parental melt REE concentrations and for assessing postcrystallization REE redistribution. Geochimica et Cosmochimica Acta, 60, 3967-3978.

Pernet-Fisher, J.F., Deloule, E., and Joy, K.H. (2019) Evidence of chemical heterogeneity within lunar anorthosite parental magmas. Geochimica et Cosmochimica Acta, 266, 109-130.

Pernet-Fisher, J.F., Joy, K.H., Martin, D.J.P., and Donaldson Hanna, K.L. (2017) Assessing the shock state of the lunar highlands: Implications for the petrogenesis and chronology of crustal anorthosites. Science Report, 7, 5888.

Phinney, W.C. (1991) Lunar anorthosites, their equilibrium melts and the bulk Moon. Proceedings of Lunar and Planetary Science Conference, 21, 29-49.

Phinney, W.C., and Morrison, D.A. (1990) Partition coefficients for calcic plagioclase: implications for Archean anorthosites. Geochimica et Cosmochimica Acta, 54, 1639-1654.

Qian, Y., Xiao, L., Head, J.W., and Wilson, L. (2021) The long Sinuous Rille system in northern Oceanus Procellarum and its relation to the Chang'e-5 returned samples. Geophysical Research Letters, 48, e2021GL092663.

Shannon, R.D. (1976) Revised effective ionic radii and systematic studies of interatomic distances in halides and chalcogenides. Acta Cryst. Sect. A32, 751–767

Shearer, C.K., Hess, P.C., Wieczorek, M.A., Pritchard, M.E., Parmentier, E.M., Borg, L.E., Longhi, J., Elkins-Tanton, L.T., Neal, C.R., Antonenko, I., Canup, R.M., Halliday, A.N., Grove, T.L., Hager, B.H., Lee, D.C., and Wiechert, U. (2006)

Thermal and magmatic evolution of the moon. Reviews in Mineralogy and Geochemistry, 60, 365-518.

Shearer, C.K., and Papike, J. (2005) Early crustal building processes on the moon: Models for the petrogenesis of the magnesian suite. Geochimica et Cosmochimica Acta, 69, 3445-3461.

Shervais, J.W., and McGee, J.J. (1998) Ion and electron microprobe study of troctolites, norite, and anorthosites from Apollo 14: Evidence for urKREEP assimilation during petrogenesis of Apollo 14 Mg-suite rocks. Geochimica et Cosmochimica Acta, 62, 3009-3023.

Shervais, J.W., and McGee, J.J. (1999) KREEP cumulates in the western lunar highlands; ion and electron microprobe study of alkali-suite anorthosites and norites from Apollo 12 and 14. American Mineralogist, 84, 806-820.

Simon, S.B., and Sutton, S.R. (2018) Valences of Ti, Cr, and V in Apollo 17 high-Ti and very low-Ti basalts and implications for their formation. Meteoritics & Planetary Science, 53, 2138-2154.

Stöffler, D., Ryder, G., Ivanov, B.A., Artemieva, N.A., Cintala, M.J., and Grieve, R.A.F. (2006) Cratering history and lunar chronology. Reviews in Mineralogy and Geochemistry, 60, 519-596.

Sun, C.G., Graff, M., and Liang, Y. (2017) Trace element partitioning between plagioclase and silicate melt: The importance of temperature and plagioclase composition, with implications for terrestrial and lunar magmatism. Geochimica et

Cosmochimica Acta, 206, 273-295.

Tepley, F.J., Lundstrom, C.C., McDonough, W.F., and Thompson, A. (2010) Trace element partitioning between high-An plagioclase and basaltic to basaltic andesite melt at 1 atmosphere pressure. Lithos, 118, 82-94.

Tian, H.C., Wang, H., Chen, Y., Yang, W., Zhou, Q., Zhang, C., Lin, H.L., Huang, C., Wu, S.T., Jia, L.H., Xu, L., Zhang, D., Li, X.G., Chang, R., Yang, Y.H., Xie, L.W., Zhang, D.P., Zhang, G.L., Yang, S.H., and Wu, F.Y. (2021) Non-KREEP origin for Chang'e-5 basalts in the Procellarum KREEP Terrane. Nature, 600, 59-63.

Togashi, S., Kita, N.T., Tomiya, A., and Morishita, Y. (2017) Magmatic evolution of lunar highland rocks estimated from trace elements in plagioclase: A new bulk silicate Moon model with sub-chondritic Ti/Ba, Sr/Ba, and Sr/Al ratios. Geochimica et Cosmochimica Acta, 210, 152-183.

Togashi, S., Tomiya, A., Kita, N.T., and Morishita, Y. (2022) Magmatic evolution of the host magma of plutonic rocks in the Procellarum KREEP Terrane. Geochimica et Cosmochimica Acta, 321, 375-402.

Warren, P.H. (1989) KREEP: Major-element diversity, trace-element uniformity (almost). In: Taylor GJ and Warren PH (eds.) Workshop on Moon in Transition: Apollo 14, KREEP, and Evolved Lunar Rocks (Technical Report 89-03), pp. 149-153. Houston: Lunar and Planetary Institute.

Warren, P.H., and Wasson, J.T. (1979) Origin of KREEP. Reviews of Geophysics, 17, 73-88.

Wieczorek, M.A., Jolliff, B.L., Khan, A., Pritchard, M.E., Weiss, B.P., Williams, J.G., Hood, L.L., Righter, K., Neal, C.R., Shearer, C.K., McCallum, I.S., Tompkins, S., Hawke, B.R., Peterson, C., Gillis, J.J., and Bussey, B. (2006) The constitution and structure of the lunar interior. Reviews in Mineralogy and Geochemistry, 60, 221-364.

Wu, S., Karius, V., Schmidt, B. C., Simon, K., and Wörner, G. (2018) Comparison of ultrafine powder pellet and flux-free fusion glass for bulk analysis of granitoids by laser ablation-inductively coupled plasma-mass spectrometry. Geostandards and Geoanalytical Research, 42, 575-591.

Wu, S., Wörner, G., Jochum, K.P., Stoll, B., Simon, K., and Kronz, A. (2019) The Preparation and preliminary characterisation of three synthetic andesite reference glass materials (ARM-1, ARM-2, ARM-3) for in situ microanalysis. Geostandards and Geoanalytical Research, 43, 567-584.

Xie, M., Xiao, Z., Zhang, X., Xu, A. (2020) The provenance of regolith at the Chang'e-5 candidate landing region. Journal of Geophysical Research: Planets, 125, e2019JE006112.

Xu, X.Q., Hui, H.J., Chen, W., Huang, S.C., Neal, C.R., and Xu, X.S. (2020) Formation of lunar highlands anorthosites. Earth and Planetary Science Letters, 536, 116138.

Xue, Z.Q., Xiao, L., Neal, C.R., Xu, Y.G., 2019. Oldest high-Ti basalt and magnesian crustal materials in feldspathic lunar meteorite Dhofar 1428. Geochimica et Cosmochimica Acta, 266, 74-108.

Yang, W., Chen, Y., Wang, H., Tian, H.C., Hui, H.J., Xiao, Z.Y., Wu, S.T., Zhang, D., Zhou, Q., Ma, H.X., Zhang, C., Hu, S., Li, Q.L., Lin, Y.T., Li, X.H., and Wu, F.Y. (2022) Geochemistry of impact glasses in the Chang'e-5 regolith: Constraints on impact melting and the petrogenesis of local basalt. Geochimica et Cosmochimica Acta, 333, 183-196.

Zhang, D, Su, B., Chen, Y., Yang, W., Mao, Q., and Jia, L.H. (2022) Titanium in olivine reveals low-Ti origin of the Chang'E-5 lunar basalts, Lithos, 106639.

Zong, K., Wang, Z., Li, J., He, Q., Li, Y., Becker, H., Zhang, W., Hu, Z., He, T., Cao, K., She, Z., Wu, X., Xiao, L., and Liu, Y. (2022). Bulk compositions of the Chang'E-5 lunar soil: Insights into chemical homogeneity, exotic addition, and origin of landing site basalts. Geochimica et Cosmochimica Acta, 335, 284-296.

Endnote:

[1]Deposit item AM-XX, Online Materials.

FIGURE CAPTIONS

FIGURE 1. Anorthite fraction variation diagrams for EPMA data of plagioclase grains from Chang'E-5 samples. (a) Histogram of the anorthite content (mol%). (b) K_2O (wt.%) versus anorthite content (mol%) for EPMA data. (c) TiO_2 (wt.%) versus anorthite content (mol%). The previously reported data for Chang'E-5 samples are from Che et al. (2021),

Hu et al. (2021) and Tian et al. (2021). The Apollo low-Ti basalts (12 and 15) and high-Ti basalts (11 and 17) are from MoonDB Research (http://search.moondb.org/). The dashed grey line in plot (c) represents the detection limit for EPMA analysis. The measured data are provided in Online Materials[1] Table OM1.

FIGURE 2. Chondrite-normalized rare earth element (REE) distribution patterns for LA-ICP-MS data for plagioclase and pyroxene grains in Chang'E-5 basaltic clasts. The normalization data are from Anders and Grevesse (1989). The data of pyroxene and plagioclase reported in Tian et al. (2021) are shown for comparison. Two plagioclases in panel (b) highlighted by an ellipse show Sm anomalies (much lower Sm concentration). This may be caused by random analytical error because these two plagioclases do not show obvious differences in terms of other trace elements. The measured data are provided in Online Materials[1] Tables OM3 and OM4.

FIGURE 3. The variation diagrams of trace elements versus anorthite content in plagioclase analyzed by LA-ICP-MS. The symbols filled with grey are from Tian et al. (2021). Error bars represent 2SE and some errors are smaller than symbols.

FIGURE 4. Results of Raman analysis for pyroxene and plagioclase from Chang'E-5 basalts separated from lunar soil CE5C0400YJFM00406. The analyzed spots are provided in Online Materials[1] Figs. OM1 and OM2.

DOI: https://doi.org/10.2138/am-2022-8570. http://www.minsocam.org/

FIGURE 5. Chondrite-normalized REE concentrations for the calculated equilibrium parental melts from the plagioclase and pyroxene compositions (Table 1). The areas filled with light blue and light red represent the ranges of chondrite-normalized melts estimated from plagioclase and high-Ca augite, respectively. The Chang'E-5 moderate-Ti glass beads from Yang et al. (2022) and the Apollo 15 KREEP basalts from supplemental material to New Views of the Moon (2006) are shown for comparison. The bulk compositions of Chang'E-5 lunar soils are from Li et al. (2022) and Zong et al. (2022). The normalization data are from Anders and Grevesse (1989).

FIGURE 6. Trace element concentrations of the parental melts estimated from Chang'E-5 plagioclase. Chemical compositions of the lunar crust represented by anorthosites are deduced from Pernet-Fisher et al. (2019). The KREEP endmember is from Warren (1989). The data source for the Apollo 15 KREEP basalts is the same as in Figure 5. Error bars represent 2SE and some errors are smaller than symbols. The data are presented in Online Materials[1] Table OM5.

FIGURE 7. (a) The TiO_2 contents of parental melt estimated from EPMA data of plagioclase shown in Figure 1c. The Ti partition coefficient between plagioclase and melt and the measured TiO_2 contents are used to back-calculate the parental melt TiO_2 contents. The literature data for Chang'E-5 samples are from Che et al. (2021), Hu et al. (2021) and

Tian et al. (2021). The Apollo low-Ti basalts (12 and 15) and high-Ti basalts (11 and 17) are from MoonDB Research (http://search.moondb.org/). (b) The average results of the Chang'E-5 data shown in plot (a). Each symbol represents an average TiO_2 content calculated for ΔAn =1 interval and the error bar denotes 1 SD (standard deviation). The data source for Apollo samples is the same as plot (a).

Table 1. The partition coefficients and the estimated trace element compositions of the Chang'E-5 basalts

Element	High-Ca augite[a]	Plagioclase[b] (An_{71}-An_{90})	Estimated parental melt from augite[c]	Estimated parental melt from plagioclase[d]
La	0.0290	0.0055-0.0267	62.6	140.2
Ce	0.0434	0.0051-0.0249	186.9	324.8
Nd	0.0839	0.0039-0.0191	130.1	184.1
Sm	0.1279	0.0027-0.0133	38.4	56.0
Eu	0.1469	1.2	2.7	4.4
Gd	0.1643	0.0018-0.0089	42.7	70.3
Tb	0.1791	0.0014-0.0070	6.8	11.3
Dy	0.1905	0.0011-0.0054	45.1	75.3
Er	0.2002	0.0007-0.0033	24.6	53.4
Yb	0.1973	0.0004-0.0021	22.0	74.1
Sr		1.6287		
Ba		0.1141		

[a] The partition coefficients for high-Ca augite are calculated using equations (1), (2), (3) and (4) (lattice strain model) presented in Dygert et al. (2014).

[b] The partition coefficients of REE (except for Eu) are calculated using equations (3), (6a), (6b) and (6c) (lattice strain model) presented in Sun et al. (2017). The Ba and Sr partition coefficients are also calculated using the equations (3), (7a), (7b) and (7c) (lattice strain model) presented in Sun et al. (2017). The augite and plagioclase studied here have different compositions, reflecting a wide range of crystallization temperatures. For simplicity, an average temperature of 1373 K was assumed for both high-Ca augite and plagioclase. Eight-fold coordinated ionic radii from Shannon (1976) are used in the lattice strain model for both high-Ca augite and plagioclase. The Eu partition coefficient is from Phinney and Morrison (1990).

[c] The parental REE concentrations are estimated using the average values of all measured augites in Tian et al. (2021) and this work (a total of 82 analyses), and the corresponding partition coefficients are listed in the first column.

[d] We first calculated the equilibrium melt composition for each sample based on the measured REE concentrations (this study and Tian et al., 2021) and the corresponding partition coefficients in the second column. Then, we took the average values for the parental melts (a total of 31 analyses).

This is the peer-reviewed, final accepted version for American Mineralogist, published by the Mineralogical Society of America.
The published version is subject to change. Cite as Authors (Year) Title. American Mineralogist, in press.
DOI: https://doi.org/10.2138/am-2022-8570. http://www.minsocam.org/

Figure 1

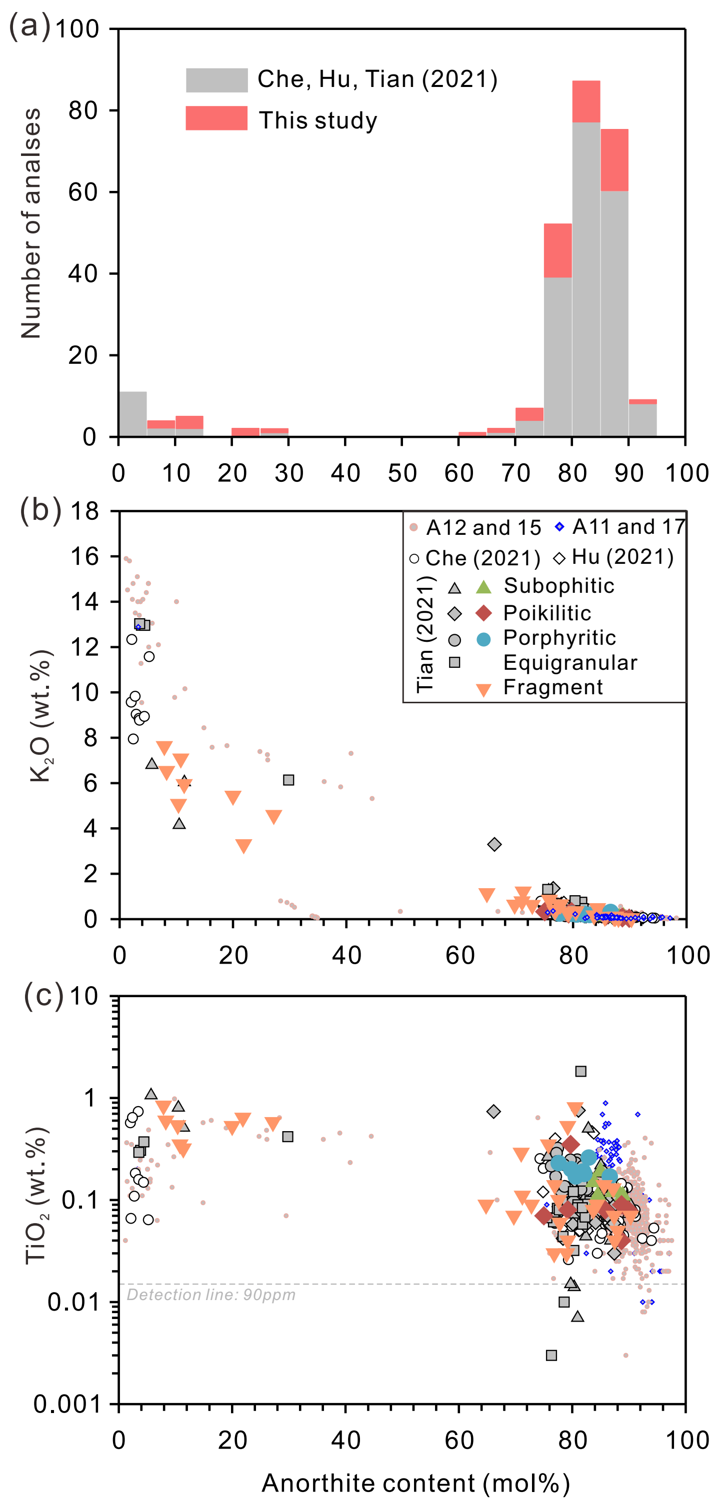

Figure 2

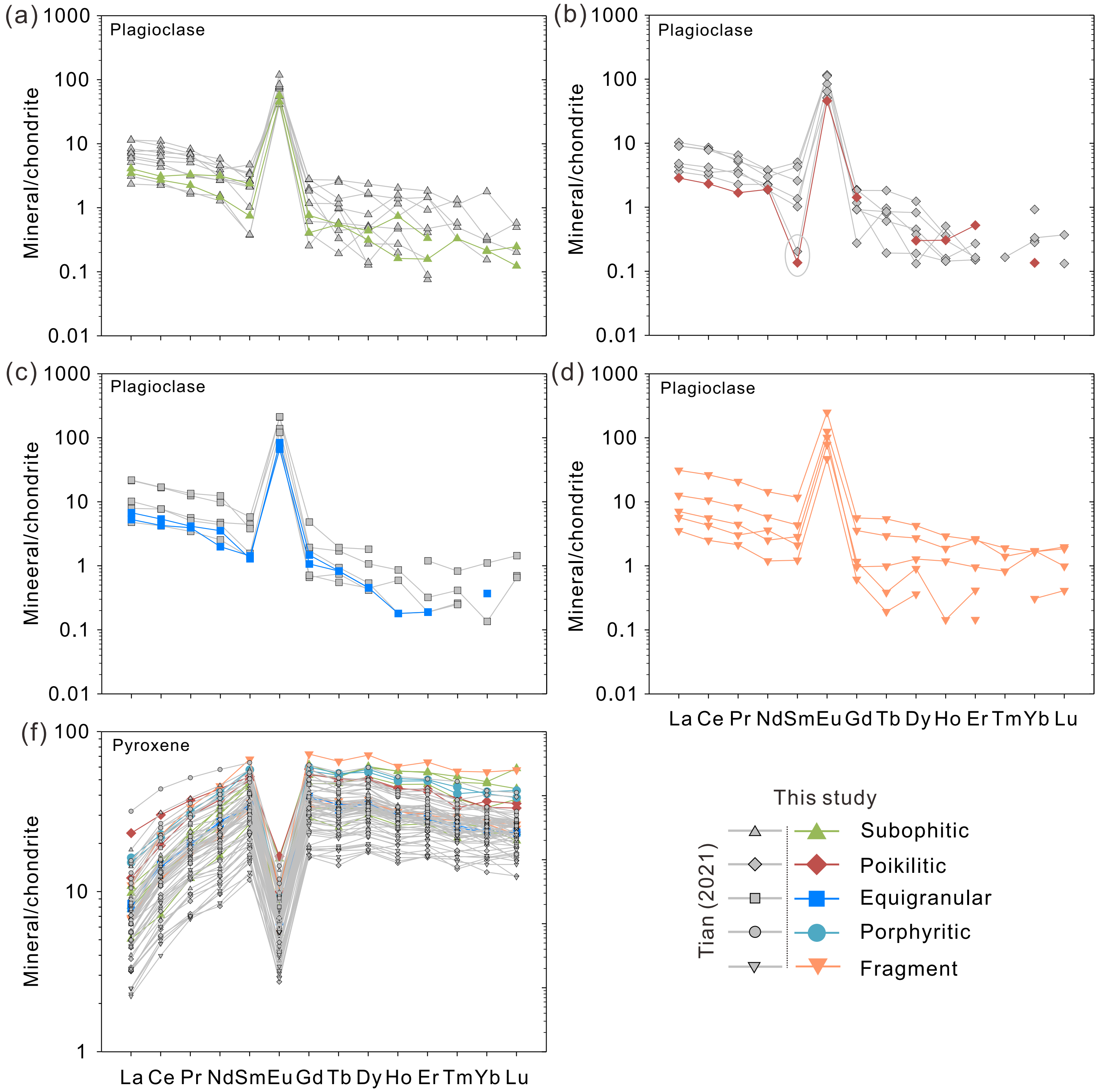
(a)
Plagioclase
Mineral/chondrite
(b)
Plagioclase
Mineral/chondrite
(c)
Plagioclase
Mineeral/chondrite
(d)
Plagioclase
Mineral/chondrite
(f)
Pyroxene
Mineral/chondrite
La Ce Pr Nd Sm Eu Gd Tb Dy Ho Er Tm Yb Lu
This study
Tian (2021)
Subophitic
Poikilitic
Equigranular
Porphyritic
Fragment

Figure 3

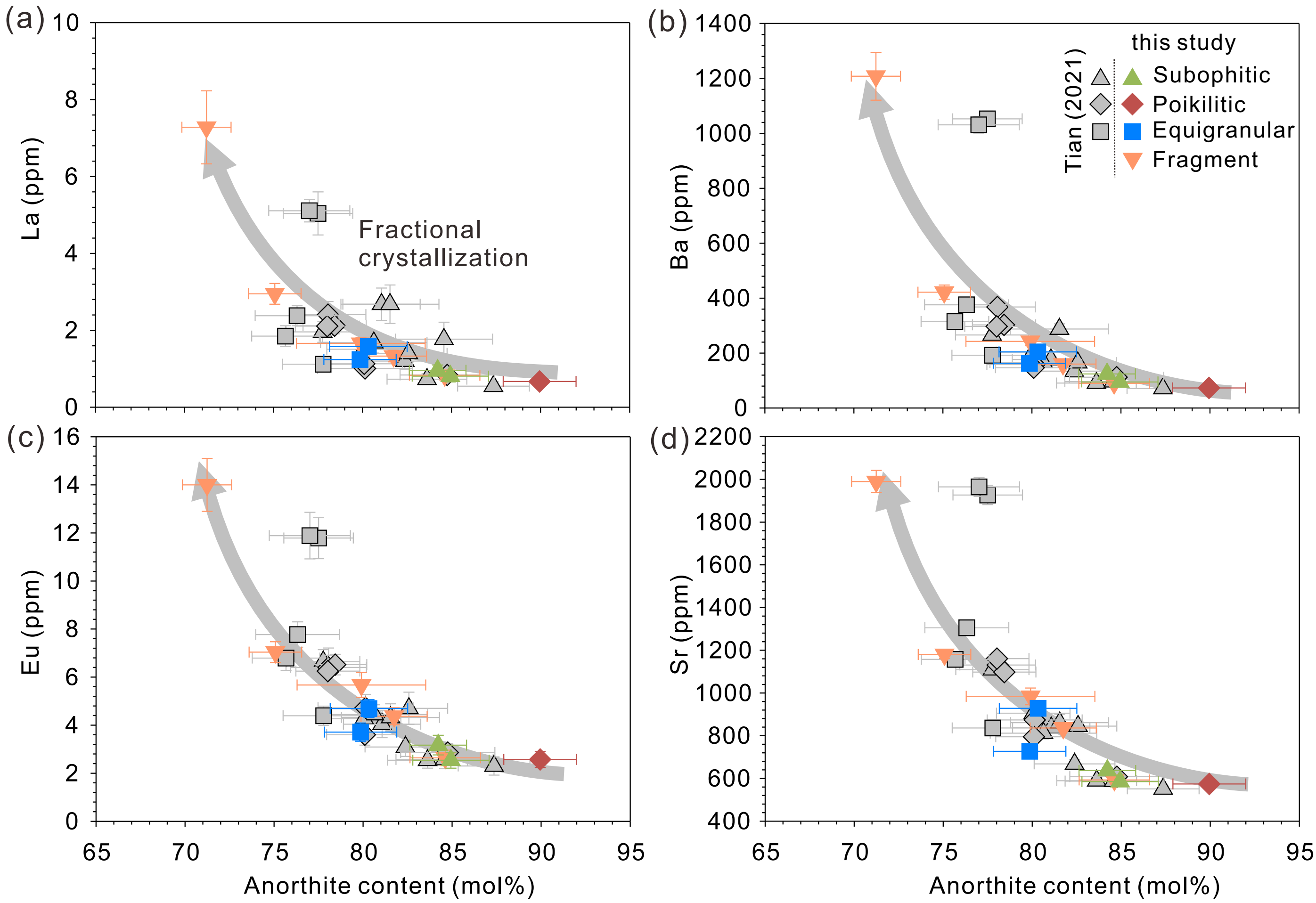
(a)
(b)
(c)
(d)
La (ppm)
Ba (ppm)
Eu (ppm)
Sr (ppm)
Fractional
crystallization
this study
Tian (2021)
Subophitic
Poikilitic
Equigranular
Fragment
Anorthite content (mol%)
Anorthite content (mol%)

Figure 4

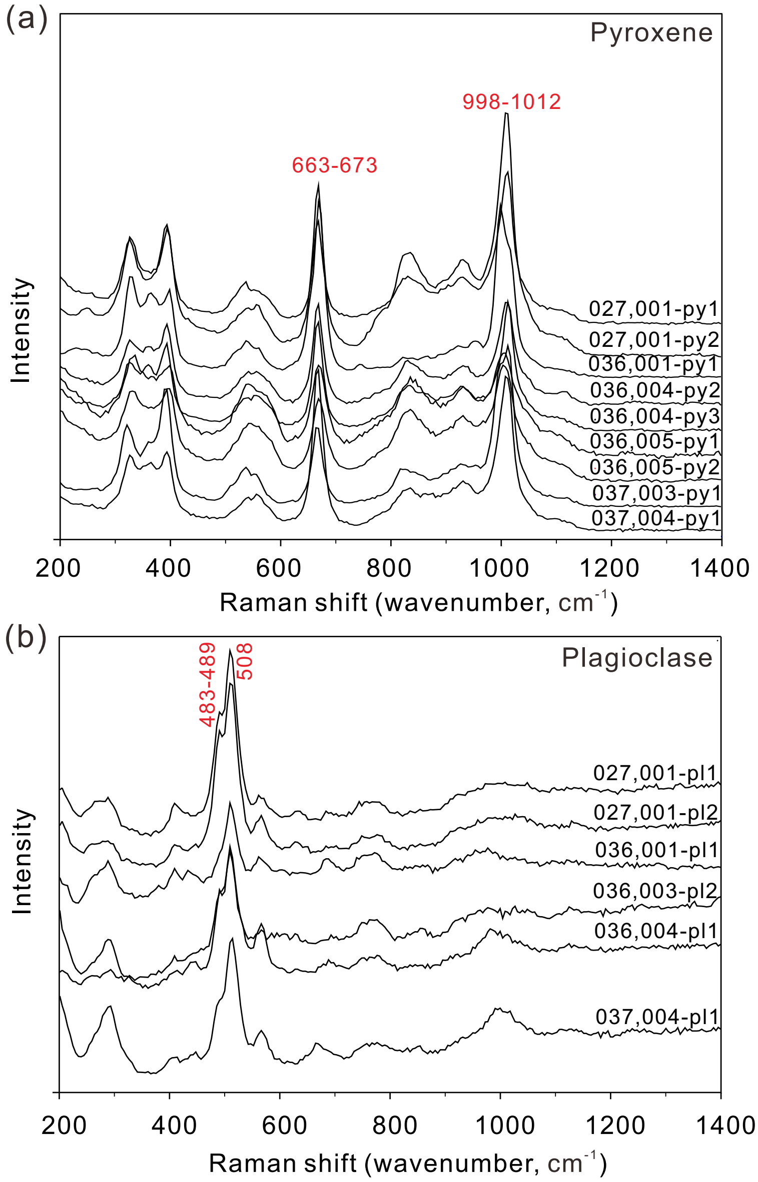
(a)
Pyroxene
998-1012
663-673
027,001-py1
027,001-py2
036,001-py1
036,004-py2
036,004-py3
036,005-py1
036,005-py2
037,003-py1
037,004-py1
Intensity
200
400
600
800
1000
1200
1400
Raman shift (wavenumber, cm-1)
(b)
Plagioclase
483-489
508
027,001-pl1
027,001-pl2
036,001-pl1
036,003-pl2
036,004-pl1
037,004-pl1
Intensity
200
400
600
800
1000
1200
1400
Raman shift (wavenumber, cm-1)

DOI: https://doi.org/10.2138/am-2022-8570. http://www.minsocam.org/

Figure 5

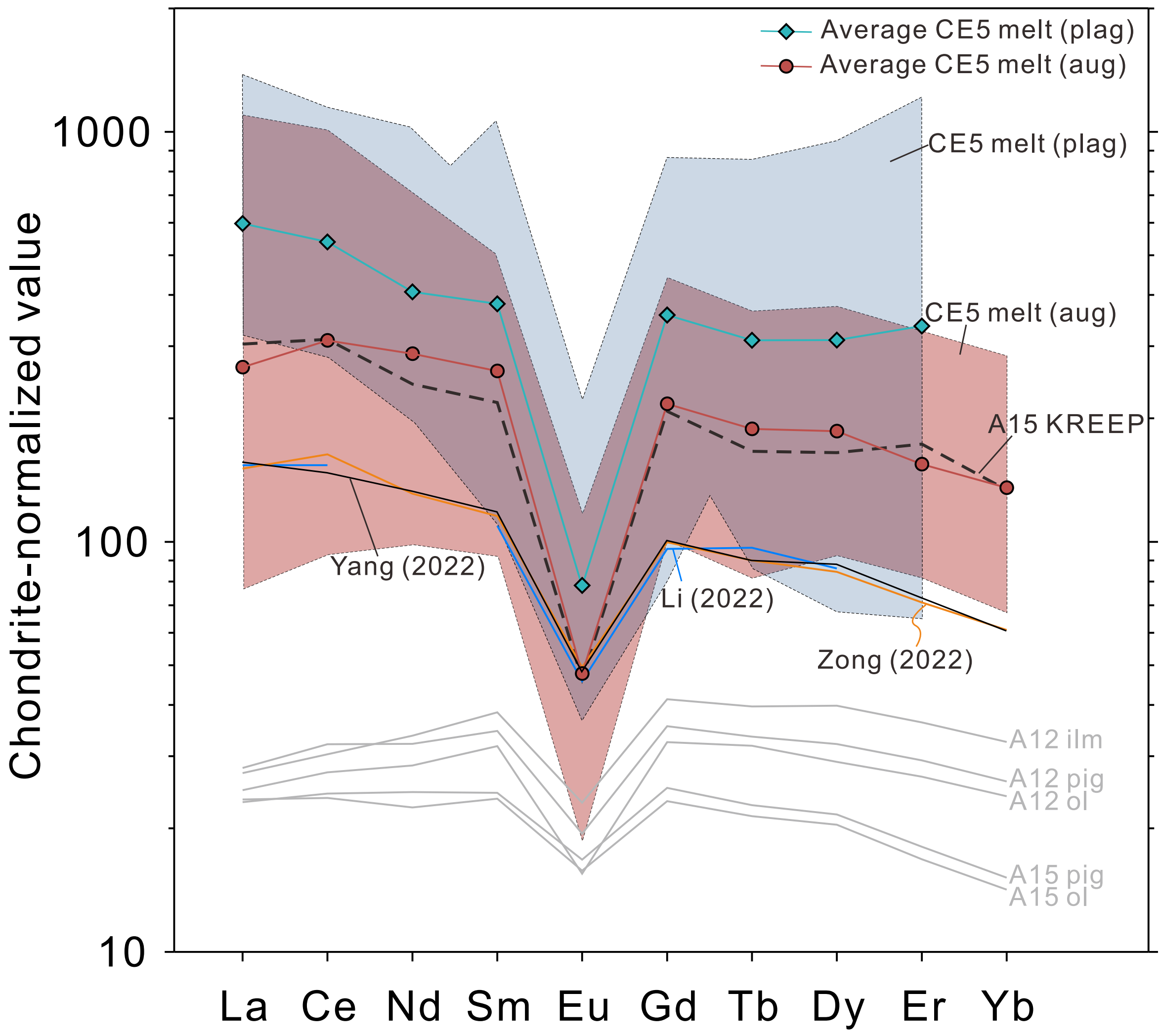

This is the peer-reviewed, final accepted version for American Mineralogist, published by the Mineralogical Society of America.
The published version is subject to change. Cite as Authors (Year) Title. American Mineralogist, in press.
DOI: https://doi.org/10.2138/am-2022-8570. http://www.minsocam.org/

Figure 6

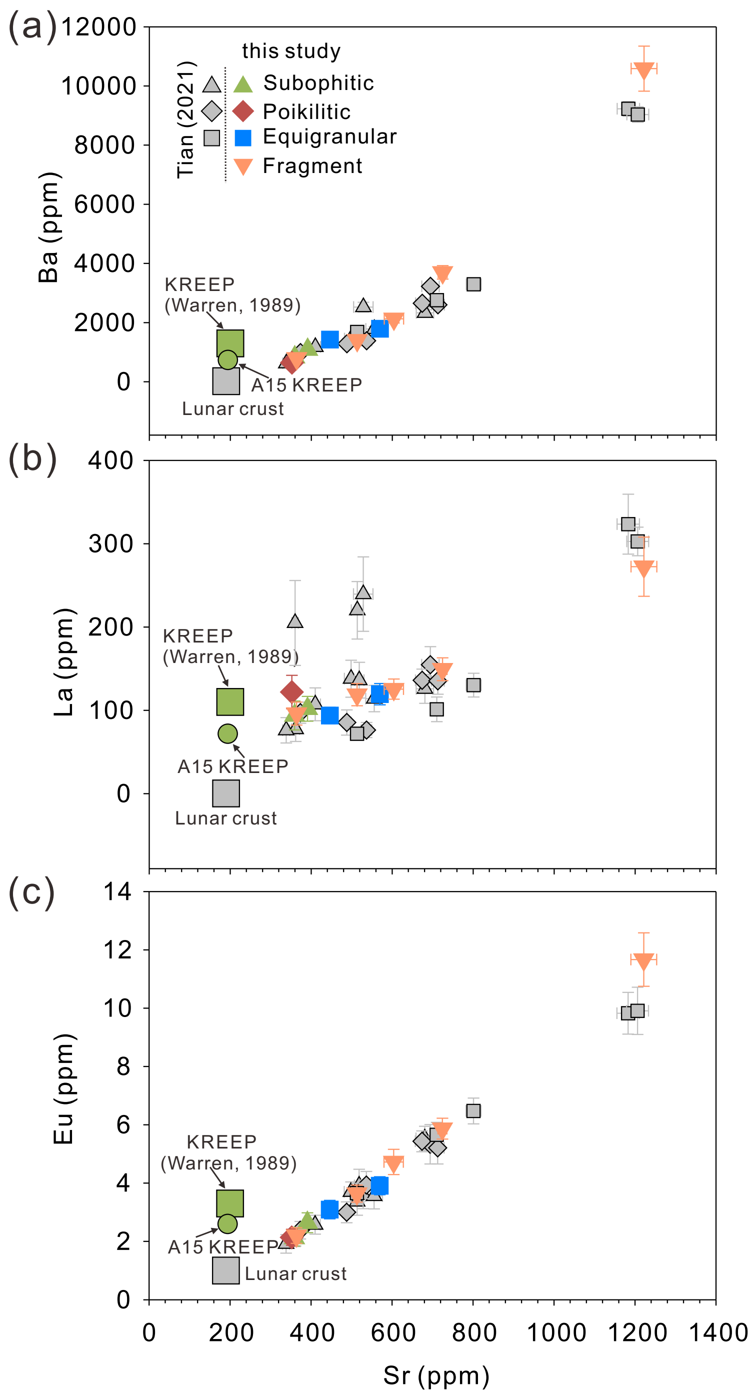

Figure 7

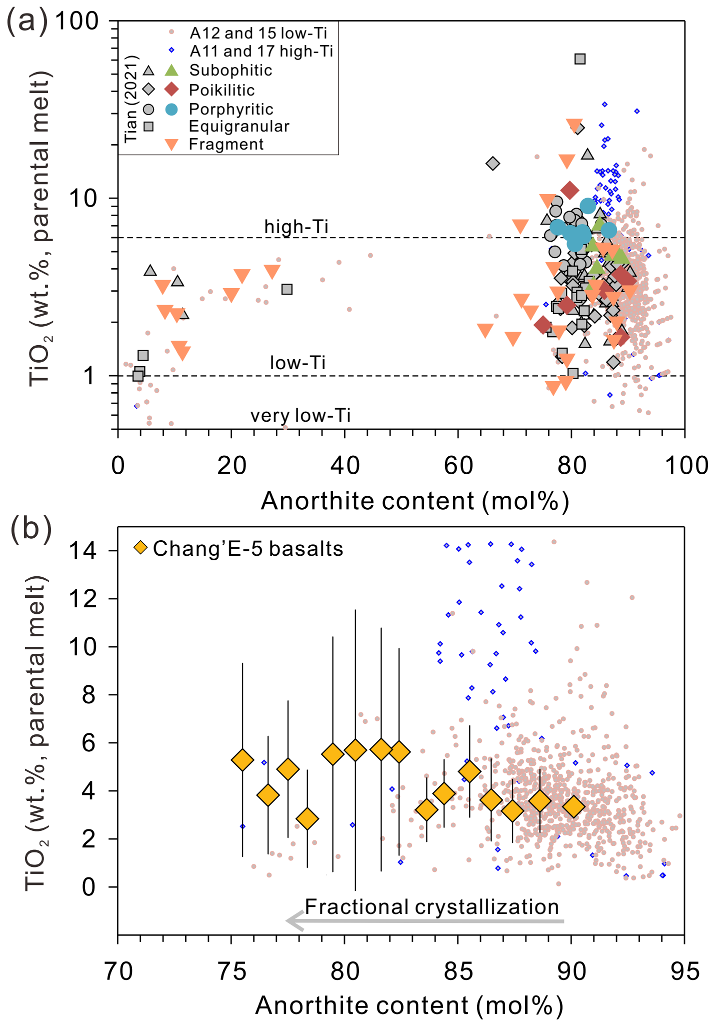
(a)
A12 and 15 low-Ti
A11 and 17 high-Ti
Tian (2021)
Subophitic
Poikilitic
Porphyritic
Equigranular
Fragment
high-Ti
low-Ti
very low-Ti
TiO2 (wt.%, parental melt)
Anorthite content (mol%)
100
10
1
0
20
40
60
80
100
(b)
Chang'E-5 basalts
Fractional crystallization
TiO2 (wt.%, parental melt)
Anorthite content (mol%)
14
12
10
8
6
4
2
0
70
75
80
85
90
95